TOPOGRAPHY OF THE TRANSITION ZONE SEISMIC DISCONTINUITIES

George Helffrich
Earth Sciences
University of Bristol
Bristol, England

Abstract. Phase transformations in mantle mineralogies probably cause the transition zone seismic discontinuities, nominally at 410, 520, and 660 km depth. Thermodynamic principles govern phase transformations, making them sensitive to changes in the mantle's ambient conditions through the thermodynamic response: Changes in temperature or composition shift the transformation to a different pressure, creating topography on a level discontinuity. With this use as an exploratory tool for the mantle in mind, we review the basic seismological and phase equilibrium concepts underlying the detection and interpretation of the seismic wave arrivals associated with the transition zone discontinuities. Reviewing the evidence for and against the phase transition model, we conclude that it is viable and describe how discontinuities have been and can be used to probe the physical and chemical state of the transition zone.

1. INTRODUCTION

1.1. Radial Earth Structure

Discontinuities separate regions of smoothly varying seismic velocity inside the Earth (Figure 1). Working outward from the Earth's center, the discontinuities are at the inner core boundary, then at the core/mantle boundary (CMB), then three midmantle discontinuities at *410*, *520*, and *660* km depth, and then the Moho at about 35 km depth. (Terms in italic are defined in the glossary, following the main text.) Two of these discontinuities, the Moho and the CMB, correspond to significant compositional changes in the stuff of the Earth: the boundary between a peridotitic mantle and an iron-rich core in the case of the CMB and between a mafic mantle and a silicic crust in the case of the Moho [*Williamson and Adams*, 1923]. This paper focuses on the mantle discontinuities in the *transition zone*, the region between about 400 and 800 km depth. Whereas in seismology's nascency new discontinuity discoveries progressively refined our basic knowledge of Earth structure, in its maturity the discontinuities themselves become investigative tools rather than investigative targets. The goal of this review is to show how changes in discontinuity depth have been and can be used to investigate the mantle's properties. The argument develops along two lines. The first establishes what the major discontinuities at 410, 520, and 660 km depth are. Significantly, the topography on the discontinuities gives strong evidence to discriminate among different ideas about how they arise. The second strand describes the sort of scientific craftsmanship that can be achieved using the spatial variation of discontinuity depths as a tool, a tool that turns out to be surprisingly versatile, under continual refinement, and increasingly common in a research seismologist's tool kit.

1.2. Detecting Discontinuities

Seismic discontinuities are detected by the additional arrivals they cause in the seismic wave field by *reflection* and *refraction* of the direct wave at the discontinuity. Reflection typically leads to an earlier arrival than would be expected in a uniform medium. Its timing relative to the direct arrival yields the discontinuity's depth. A refraction usually leads to more than one arrival, where only one would be expected in a uniform medium. In this case, one deduces the discontinuity depth from the distance from the seismic source where the multiple arrivals appear. The Earth's major discontinuities were initially discovered this way, and others continue to be discovered like this [*Oldham*, 1906; *Lehmann*, 1936; *Song and Helmberger*, 1998].

There are quite diverse methods for measuring discontinuity depths, probably best described through sketches (Figure 2) (see *Shearer* [1991] for more exotic ones). One way to characterize the methods is by the position where the seismic wave interacts with the discontinuity: near the *source*, near the *receiver*, or elsewhere. Near-source studies provide the best spatial resolution because there is little opportunity for the seismic wave field to spread out before interacting with the discontinuity (its *Fresnel zone* width is small). Spatial resolution for near-receiver studies is worse since the interaction is at least 410 km from the receiver. Interac-

Reviews of Geophysics, 38, 1 / *February 2000*
pages 141–158
8755-1209/00/1999RG000060*$15.00*
Paper number 1999RG000060

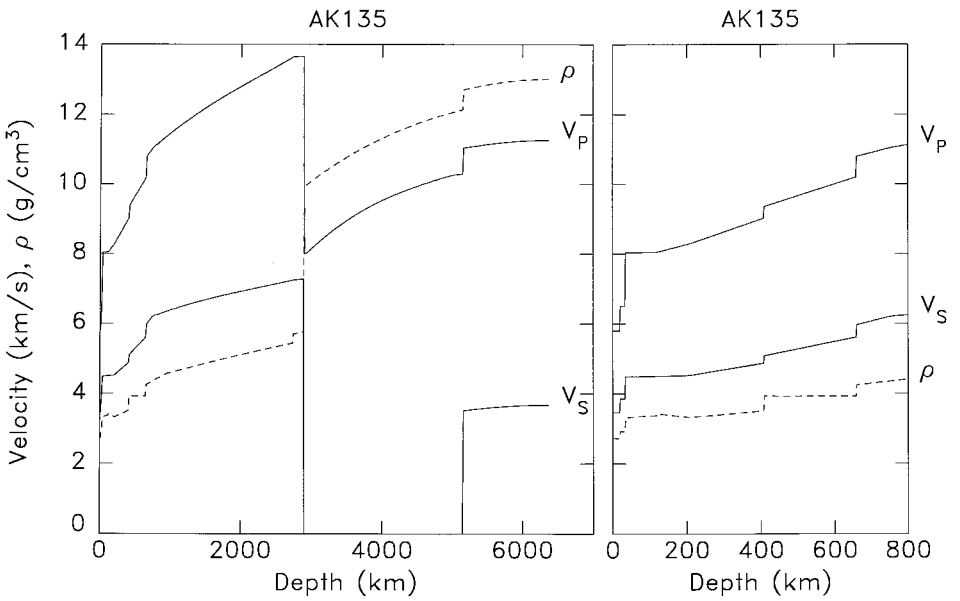

Figure 1. *P* and *S* wave speed and density profile in the Earth [*Kennett et al*., 1995]. Jumps at 410 and 660 km depth demark the transition zone discontinuities. Right panel provides an expanded view of the Earth's upper 800 km, which includes the transition zone. The 520 is not featured in this model.

tions elsewhere in the mantle have correspondingly poorer spatial resolution.

Seismic wave frequency affects the size of the Fresnel zone and thus its spatial resolution. Figure 3a diagrams the Fresnel zone of the near-receiver conversion *P*660*s*. Its Fresnel zone is ~500 km wide at the discontinuity, blunting its ability to resolve narrow structures. In contrast, Figure 3b shows the near-source conversion *S*660*P* for an earthquake at 500 km depth. Its 100- to 200-km Fresnel zone at the 660 arises due to the proximity of the source to the discontinuity under study. With a narrower probe of the discontinuity, correspondingly smaller scale structure is visible (as suggested by larger reported topography using short-period studies, to be discussed below).

2. NATURE OF THE 410, 520, AND 660

The enduring idea that discontinuous changes in wave speeds in the transition zone correspond to *phase* changes in mantle minerals arose almost simultaneously with the discovery of the discontinuities. On April 24, 1936, H. Jeffreys read a paper on seismic velocities in the mantle in which he noted that the kinks in travel time curves at 20° epicentral distance marked discontinuous changes in seismic wave speeds. In the discussion that followed, J. D. Bernal reminded the audience that V. M. Goldschmidt's work on the germanate analog to the silicate mineral olivine underwent pressure-mediated *phase transitions* to denser structures. Bernal speculated that the discontinuous increases in seismic wave speeds could be due to changes in the structure of olivine brought about by pressure increasing with depth in the Earth [*Bernal*, 1936]. The transition zone could represent a broad transition, mixing material with low-pressure properties and high-pressure ones [*Meijering and Rooymans*, 1958].

In contrast, *Williamson and Adams* [1923] argued for a varying composition with depth. In their proposed Earth structure the greatest departure from the contemporary view was a gradual change in composition below about 1600 km depth through a mixed silicate and iron region. Below the shallow crust's silica-rich layer and above this mixed region, they found that self-compression of material at constant composition explained best the density profile they inferred from the seismic travel time tables available at the time. *Birch* [1952, 1961] reexamined this idea later, and while he did not rule out compositional changes as a possibility, he was not a proponent for two reasons. First, there was a contradiction between transition zone thermal gradients inferred from the seismic velocity structure and from mantle heat flow. Second, a compositional change violated the then known velocity-density systematics developed by *Birch* [1961]. *Ringwood*'s [1958a, b] experiments on the silicate olivine polymorphs yielded an appropriate seismic wave speed and density for transition zone material. The simplest explanation lay in attributing the transition zone velocity gradients to phase changes rather than to compositional changes.

These two views framed the debate vigorously pursued by the seismology and mineral physics communities until quite recently. The crucial test to distinguish between the competing ideas arose among those studying the way the discontinuities influence mantle convection [*Christensen and Yuen*, 1984; *Kincaid and Olson*, 1987].

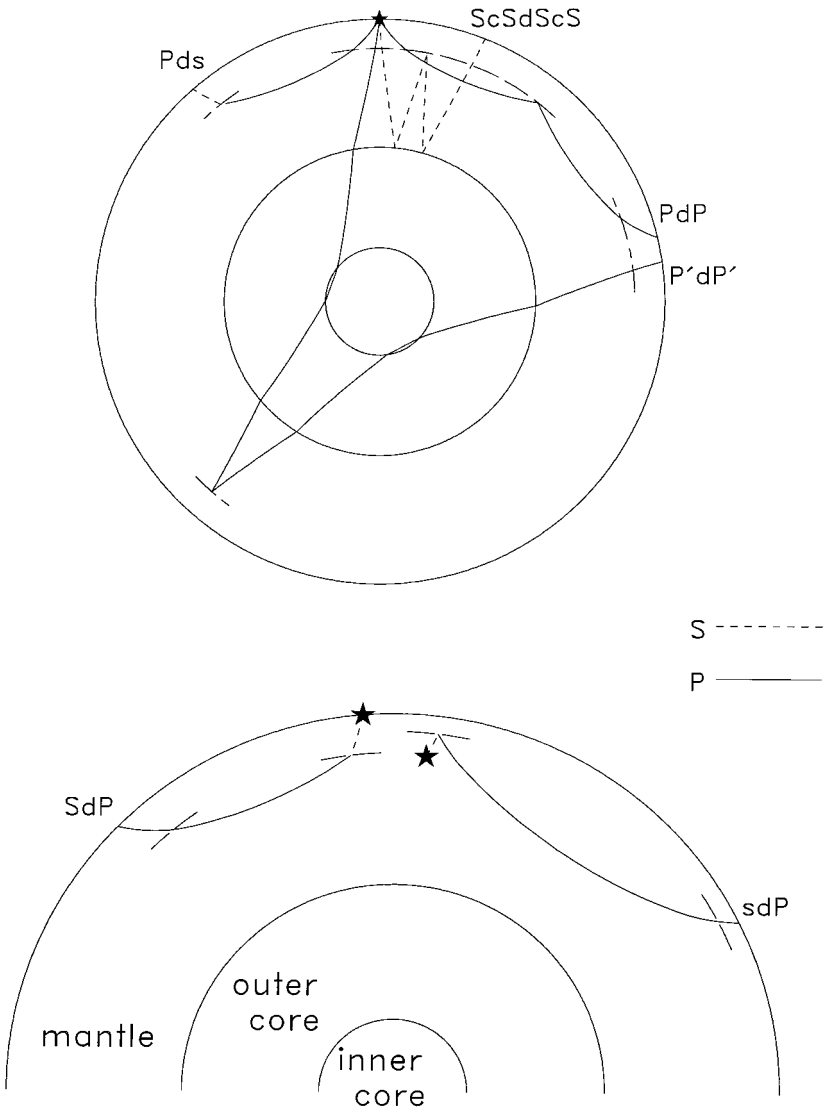

Figure 2. Seismic wave interaction geometries with the discontinuities in the transition zone. *P* (solid lines) and *S* (dashed lines) ray paths leave source (stars) and reflect off or convert type at discontinuity (long-dashed line). The interactions illustrated in the top panel take place either near the receiver (*Pds*) or midway between the source and receiver (*ScSdScS*, *P′dP′*, *PdP*). The bottom panel shows the interactions that occur near the source (*SdP* and *sdP*).

Any mass flux through a discontinuity will entrain a halo of surrounding material with it. If the discontinuity is compositional, the body moving through it will not readily mix with the material on the other side of the discontinuity due to its high viscosity. Therefore the discontinuity will bulge downward or upward in the direction of mass flux. Alternatively, if the discontinuity results from a phase change, the thermodynamic parameters governing the phase change dictate the discontinuity's position. Provided that heat can diffuse in or out of the region at rates comparable to material motion, and that metastability does not play a role, the discontinuity will adopt its equilibrium position in the mantle, moving upward or downward either with or against the mass flux position. These are the conditions that prevail in the mantle [*Jeanloz and Thompson*, 1983; *Katsura and Ito*, 1989; *Ito and Takahashi*, 1989].

Another way to discriminate between the two discontinuity explanations is to compare the observed seismic characteristics with ones calculated from the material properties of the substances supposedly lying athwart the discontinuity. The seismic observables are the reflection amplitudes from the discontinuity as a function of frequency. This approach requires both good material property data (density, *P* wave speed, and *S* wave speed) and thermodynamic data (to calculate the discontinuity's thickness or transformation interval in pressure), the province of mineral physics, experimental petrology, and solid solution modeling. The combined uncertainty from these three sources leads to greater uncertainty in the

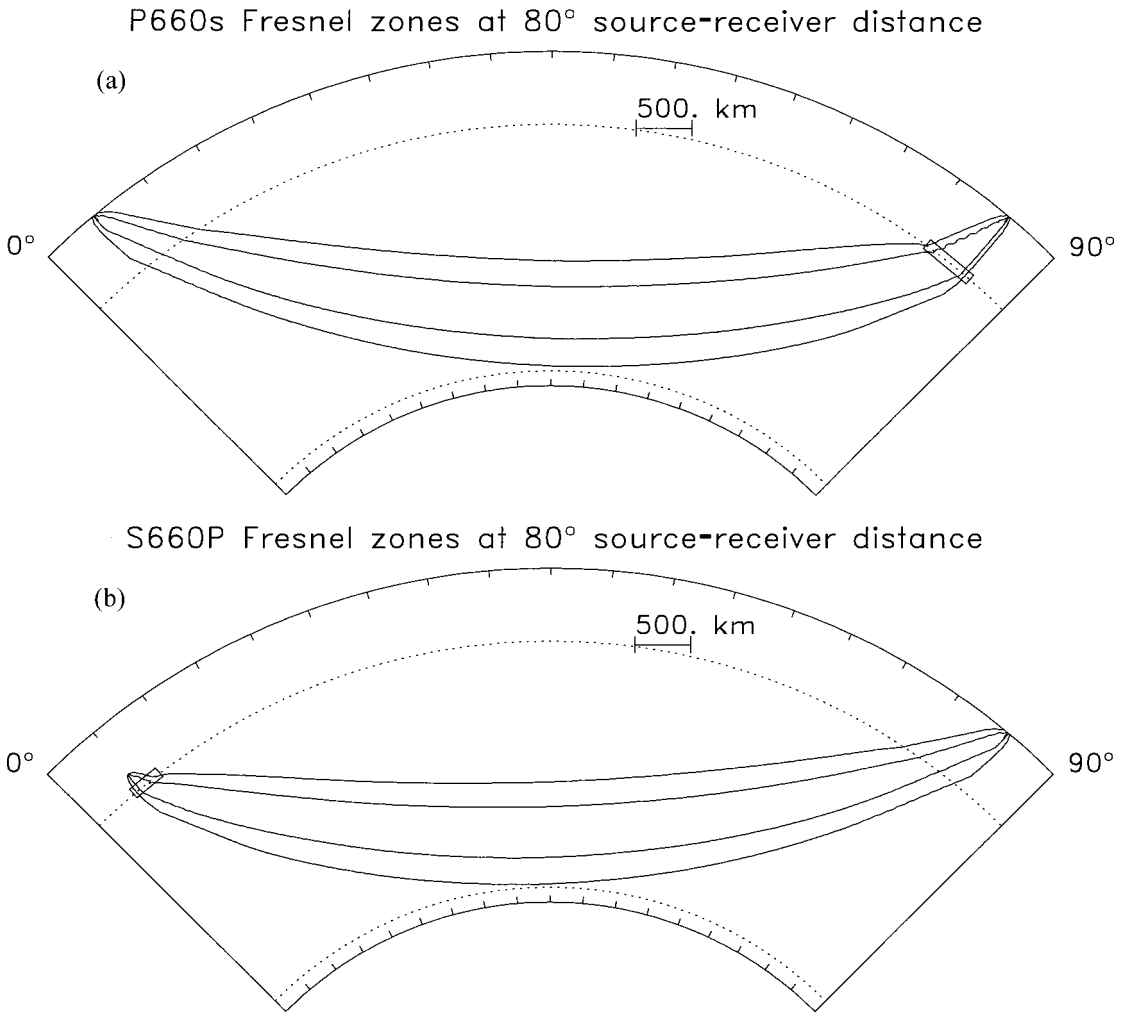

Figure 3. Quarter-period Fresnel zones for two interactions, one near the source and one near the receiver. Regions enclose 5- (narrower) and 20-s-period (wider) Fresnel zones. The zone is fully three-dimensional, with a width in and out of the paper about the same as the vertical height. Boxed region in each panel indicates the Fresnel zone footprint on the discontinuity. (a) The near-receiver interaction *P*660*s* averages discontinuity properties over about 400–600 km spatially, depending on the wave's frequency. (b) The near-source interaction *S*660*P* averages discontinuity properties over a smaller range, ~150 km, chiefly because the source is closer to the discontinuity under study.

overall result. Approaches that compare calculated and observed seismic wave speeds or the calculated and observed wave speed jumps at discontinuities are not yet able to discriminate between a compositional and a phase transition origin for them [*Ita and Stixrude*, 1992; *Vacher et al*., 1998].

3. EVIDENCE AGAINST THE DISCONTINUITIES AS PHASE CHANGES

3.1. Transition Interval Too Broad

Virtually all mantle minerals ($(Mg, Fe)_2SiO_4$ olivine, $(Mg, Fe)_2Si_2O_6$ and $Ca(Mg, Fe)Si_2O_6$ orthopyroxene and clinopyroxene, $(Ca, Mg, Fe)_3Al_2Si_3O_{12}$ garnet, (Mg, Fe)O magnesiowustite, and $(Mg, Fe)SiO_3$ and $CaSiO_3$ perovskite) are solid solutions of two or more end-member components, predominantly an iron one and a magnesium one with a limited admixture of a calcium and an aluminum end-member in perovskite. Thus any reaction between two phases inescapably leads to a pressure-temperature region where both product and reactant coexist (a consequence of the phase rule [*Ferguson and Jones*, 1966]). This means that every phase change in the Earth's mantle will progress through a zone of transitional seismic properties interpolating those above and below the phase change [*Bina and Wood*, 1987]. This is seismically observable. The amplitude of reflections off of a gradient in seismic properties depends on the ratio of the width of the transitional region to the *wavelength* of the seismic wave interacting with it. Detectable reflections only arise from thin gradient zones relative to the wavelength: a quarter wavelength or less [*Richards*, 1972]. Since there are visible

reflections from the 410- and the 660-km discontinuities when illuminated with *short-period* seismic waves (~2 s, corresponding to wavelengths of 18–20 km in the transition zone) [*Engdahl and Flinn*, 1969; *Whitcomb and Anderson*, 1970; *Adams*, 1971; *Teng and Tung*, 1973; *Sobel*, 1978; *Nakanishi*, 1986; *Wajeman*, 1988; *Nakanishi*, 1988; *Vidale and Benz*, 1992; *Benz and Vidale*, 1993; *Petersen et al*., 1993; *Yamazaki and Hirahara*, 1994; *Vidale et al*., 1995; *Collier and Helffrich*, 1997; *Xu et al*., 1998], both these discontinuities must be sharp: 4–5 km in vertical extent, corresponding to a pressure interval of about 0.15 GPa.

The reactions taking place between ~400 and ~700 km depth involving the $(Mg, Fe)_2SiO_4$ component in mantle minerals are

$$\text{(R1)}\quad \underset{\text{olivine }(\alpha)}{(Mg, Fe)_2SiO_4} = \underset{\text{wadsleyite }(\beta)}{(Mg, Fe)_2SiO_4} \qquad (400\text{ km}),$$

$$\text{(R2)}\quad \underset{\text{wadsleyite }(\beta)}{(Mg, Fe)_2SiO_4} = \underset{\text{ringwoodite }(\gamma)}{(Mg, Fe)_2SiO_4} \qquad (520\text{ km}),$$

$$\text{(R3)}\quad \underset{\text{ringwoodite }(\gamma)}{(Mg, Fe)_2SiO_4} = \underset{\text{magnesiowustite}}{(Mg, Fe)O} + \underset{\text{perovskite}}{(Mg, Fe)SiO_3} \qquad (700\text{ km}).$$

There are other reactions involving garnet which progress over a broader depth range and do not contribute to discontinuous seismic wave speed changes:

$$\text{(R4)}\quad \underset{\text{clinopyroxene}}{2Ca(Mg, Fe)Si_2O_6} = \underset{\text{in garnet}}{(Ca_{2/3}(Mg, Fe)_{1/3})_3((Mg, Fe)_{1/2}, Si_{1/2})_2Si_3O_{12}} \qquad (300\text{–}500\text{ km}),$$

$$\text{(R5)}\quad \left.\begin{array}{l} \underset{\text{in garnet}}{Ca_3(Ca_{1/2}Si_{1/2})_2Si_3O_{12}} \\ = \underset{\text{perovskite}}{4CaSiO_3} \\ \underset{\text{in garnet}}{(Mg, Fe)_3((Mg, Fe)_{1/2}(Al, Si)_{1/2})_2Si_3O_{12}} \\ = \underset{\text{perovskite}}{4(Mg, Fe)(Si, Al)O_3} \end{array}\right\} (700-800\text{ km}).$$

Early experimental results and thermodynamic modeling could not reconcile the transition interval calculated from the experimentally determined properties of (R1) and (R3) with the observed discontinuity sharpness [*Jeanloz and Thompson*, 1983; *Lees et al*., 1983; *Bass and Anderson*, 1984; *Jeanloz*, 1991; *Stixrude et al*., 1992]. The conclusion was that one or more discontinuities marked a compositional change in the mantle.

3.2. Responses of the 410 and 660 to Temperature Change Inconsistent With the Phase Transition Hypothesis

Thermodynamic principles govern all types of chemical reaction, polymorphic (as in the case of (R1) and (R2)) or heterogeneous (reactions (R3)–(R5)). One consequence is that the change in reaction position in response to pressure (P) or temperature (T) change is given by its Clapeyron slope, dP/dT. The slope is the trajectory of the boundary in P-T space separating a reaction's products and reactants when all have fixed compositions. The Clapeyron slope's definition,

$$\frac{dP}{dT} = \frac{\Delta S}{\Delta V}, \tag{1}$$

provides one way of calculating the slope through the entropy of reaction ΔS and volume ΔV, both computable from the thermodynamic properties. Alternatively, phase equilibrium experiments augmented by other thermodynamic constraints yield estimates of the Clapeyron slope [*Akaogi et al*., 1989; *Chopelas et al*., 1994; *Morishima et al*., 1994; *Bina and Helffrich*, 1994]. Virtually all determinations of the Clapeyron slope for (R1) and (R2) are positive, whereas for (R3) they are negative. Thus (R1) and (R2) move to lower pressures in colder parts of the mantle while (R3) moves to higher pressures.

Solid solutions complicate matters because (1) no longer formally holds. There is no single boundary separating products and reactants, but rather two bordering the sides of a two phase region (see Figure 4). From a practical seismological viewpoint one can retain the convenience of a formula like (1) that relates a change in discontinuity depth (or pressure, equivalently) to a temperature change through the idea of a seismic Clapeyron slope [*Helffrich and Bina*, 1994]. A two-phase region will nonetheless reflect or transmit a seismic wave, so one converts the arrival time to the position of a fictitious step-like discontinuity. This position depends on the shape of the two-phase region and on the wave's frequency due to the quarter-wavelength rule mentioned earlier. For broader transition intervals like (R1) and (R2) the difference between a thermodynamic and a seismic slope may be significant but may be neglected for a narrow one like (R3). For example, for (R1) the Mg_2SiO_4 end-member Clapeyron slope is 3.2 MPa K^{-1}, and for (R2) it is 5.3 MPa K^{-1} using data and methods from *Helffrich and Wood* [1996]. In contrast, the seismic Clapeyron slope for mantle olivine composition ($(Mg_{0.9}, Fe_{0.1})_2SiO_4$) is equal or lower and depends on frequency and marginally on incidence angle (Table 1). Longer wavelengths yield shallower slopes depending on the velocity gradient's form through the two-phase region. P-to-S conversions of throughgoing waves and the longest wavelength reflections show the largest differences.

A strong test of the idea that the 410 and 660 involve phase transformations is to examine a part of the mantle

TABLE 1. Seismic Clapeyron Slopes for Reactions (R1) and (R2) for Different Interactions

Angle, deg	*PdP, pdP, Hz*		*SdS, Hz*		*sdP, Hz*		*Pds, Hz*		*Sdp, Hz*	
	0.2	*0.05*	*0.2*	*0.05*	*0.2*	*0.05*	*0.2*	*0.05*	*0.2*	*0.05*
					$\alpha \rightarrow \beta$, *Reaction (1), 410*					
0	3.21	3.15	3.20	3.21	3.20	3.19	3.19	2.15	3.19	2.15
10	3.22	3.16	3.20	3.21	3.21	3.18	3.18	2.20	3.21	2.22
20	3.22	3.14	3.20	3.20	3.21	3.18	3.20	2.15	3.20	2.31
30	3.22	3.10	3.21	3.20	3.21	3.14	3.21	2.24	3.22	2.76
					$\beta \rightarrow \gamma$, *Reaction (2), 520*					
0	4.95	5.54[a]	5.11	5.29			NO			
10	4.94	5.43[a]	5.11	5.29			NO			
20	4.94	5.33[a]	5.12	5.28			NO			
30	4.92	5.73[a]	5.13	5.24			NO			
40	4.92	5.93[a]	5.15	5.20			NO			

Slopes are given in MPa K^{-1}. Uncertainty in all slopes is ± 0.05 MPa K^{-1}. Subregular solution interaction parameters are W^{β}_{MgFe} −2 kcal, W^{β}_{FeMg} +4 kcal, W^{γ}_{MgFe} +3 kcal, W^{γ}_{FeMg} +5 kcal, for mixing on two sites. Reaction (R2) seismic properties are estimated from 1% *P* and *S* wave speed increases and 1.5% density increase through the transition region [*Rigden et al*., 1991; *Jones et al*., 1992], which give reflected amplitudes of ~1% of the incident wave [*Shearer*, 1990, 1991]. NO, not observable.

[a]Complex wave forms have ± 0.3 MPa K^{-1} uncertainty.

where the temperature varies laterally and see how the discontinuities behave. Subduction zones are ideal. No matter what the boundary conditions are at the subducted slab/mantle interface, the thermal inertia of the slab will lead to substantial (up to 1000 K) temperature differences between mantle and slab interior [*McKenzie*, 1969; *Furukawa*, 1994], leading to displacements of 30–90 km from the normal discontinuity depth (for respective slopes of (R1) around 3.1 MPa K^{-1} and of (R3) around −2 MPa K^{-1}). Thus the 410 should get shallower and the 660 should get deeper where radial temperature variations exist in the mantle, and 410 uplift should be ~50% larger than 660 depression.

One set of observations used to test the phase transformation idea are underside reflections of *P* and *S* waves from the discontinuity, *PdP* or *SdS* (Figure 2). *Shearer* [1991, 1993] investigated the discontinuities globally in this way, including a detailed examination around a northwestern Pacific subduction zone, and found that the 660 lies deeper but the 410 neither deepens nor shallows significantly. Globally, 660 depths vary more than 410 depths. Using a similar *long-period* method based on *precursors* to multiply reflected *ScS* (*ScSdScS*; Figure 2), *Revenaugh and Jordan* [1991] found ±15 km 660 deflection but ±10 km 410 deflection away from subduction zones. Probing subduction zones using short-period waves, *Vidale and Benz* [1992] found similarly larger 660 deflection than 410 deflection, but the ~25-km 660 depression coincided with ~10-km uplift on the 410. In sum, the results suggest that the 660 moves more than the 410 does, with larger shifts in position inferred using short-period waves.

Other investigators approached the problem more schematically, asking whether 410 depth variations were positively or negatively correlated with 660 ones [*Revenaugh and Jordan*, 1991; *Stammler and Kind*, 1992; *Stammler et al*., 1992; *Clarke et al*., 1995; *Chevrot et al*., 1999]. Verdicts are mixed. *Revenaugh and Jordan* [1991] and *Clarke et al*. [1995] find them anticorrelated, but *Stammler et al*. [1992] and *Stammler and Kind* [1992] do not. These observations do not always conform to the behavior expected from a pair of reactions with oppositely signed Clapeyron slopes responding to mantle temperature changes. One discontinuity should rise and the other should deepen, and the 410's deflection should be greater than the 660's.

4. EVIDENCE SUPPORTING DISCONTINUITIES AS PHASE CHANGES

4.1. Sharp Transitions Possible Through Thermodynamic Modeling

One objection to the phase transition model for the transition zone discontinuities is that they are seismically too thin. Both the 410 and 660 are sharp discontinuities because they are observed at short *periods*. Sharpness is a thermodynamic property of the phase transition deriving from the form of the phase diagram [*Bina and Wood*, 1987] (Figure 4), but seismic estimates can lead to narrower inferred transition intervals [*Helffrich and Bina*, 1994]. The transition width is the extent in pressure of the two-phase region separating the products and reactants, which in turn depends on the slope of the boundaries separating one- and two-phase regions. The compositions of the coexisting phases must be determined by experiment to construct the phase diagram or, equivalently, a solid solution model proposed that specifies the compositions of the coexisting phases given pressure and temperature.

While coexisting phase compositions may be determined accurately by electron probe microanalysis, con-

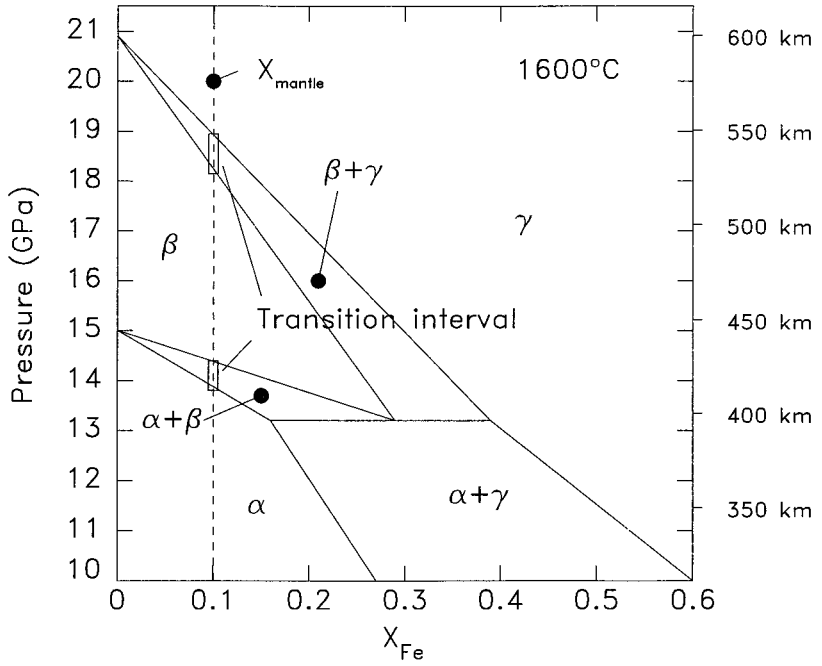

Figure 4. Schematic phase diagram of the Mg_2SiO_4–Fe_2SiO_4 system at constant temperature, showing one-phase regions (α, β, γ) and two-phase regions (α + β), (α + γ), (β + γ) of coexisting phases at a given pressure. Different slopes to the lines bounding the two-phase regions control the transition interval thickness (boxed regions), which can be made broad or thin. X_{mantle} is mantle olivine's Fe content.

straining experimental pressure and temperature is difficult due to the differences in high-pressure scales [*Jeanloz and Thompson*, 1983; *Helffrich and Wood*, 1996; *Irifune et al*., 1998; *Gudfinnsson and Wood*, 1998] and high thermal gradients in any experimental apparatus. When processing experimental data to develop either a phase diagram or a solid solution model, *P* or *T* uncertainty permits vertical shifting of the data but composition is comparatively fixed. Thus the same partitioning data may be compatible with either a broad or a narrow transition interval within their pressure or temperature uncertainties. On this account it should not be surprising to find feasible thermodynamic models yielding narrow transition intervals and thus a sharp 410 discontinuity [*Wood*, 1990; *Helffrich and Wood*, 1996], even if not all experiments obviously show them. Some experiments do yield extremely narrow transition intervals [*Fei and Bertka*, 1996; *Irifune and Isshiki*, 1998], and the trend with time is for experimentally determined transition intervals to narrow, presumably due to technical advances in large-volume, high-pressure techniques [*Katsura and Ito*, 1989; *Ito and Takahashi*, 1989; *Wood and Rubie*, 1996].

4.2. Sharp Transitions Possible Through Compositional Frustration of Phase Transitions

Another effect that leads to thin transition intervals is compositional truncation of a two-phase loop by bulk composition constraints. In the dominantly three-component MgO–FeO–SiO_2 system that encompasses the bulk of mantle mineralogy, one can show the phase proportions using a ternary diagram (Figure 5). The mantle's mineralogical proportions, olivine + pyroxene + garnet in the transition zone, must add up to its bulk composition. With increasing depth or pressure, when crossing into the olivine α-β transition interval, the mantle's pyrolitic composition [*Ringwood*, 1975] is surrounded by garnet/clinopyroxene, α-olivine, and β-wadsleyite. Increasing pressure enrichens the minerals in Mg, shifting the tie lines leftward in Figure 5. There is a limit, however: The tie lines between coexisting phases must bracket the mantle's bulk composition. The point at which the leftward sweeping garnet-β tie line crosses the mantle's composition is the point all α is reacted to β. Thus even what would appear to be a broad transition interval could be narrowed by compositionally frustrating the full reaction interval in the pure olivine system [*Jeanloz and Thompson*, 1983; *Stixrude*, 1997]. Realistically, this probably does not apply to (R1) because the 410 sometimes is visible and sometimes is not [*Paulssen*, 1988; *Wajeman*, 1988; *Benz and Vidale*, 1993], whereas the 660 rarely shies away from detection (one no-show case is given by *van der Lee et al*. [1994]). Because the 410 broadens and becomes less reflective at lower temperatures [*Helffrich and Bina*, 1994], a plausible explanation for variable 410 visibility is that it becomes harder to see when uplifted. However, if the 410's sharpness were due to a compositional frustration, it should be sharp and visible everywhere. Otherwise we must invoke lateral variations in transition zone bulk composition to

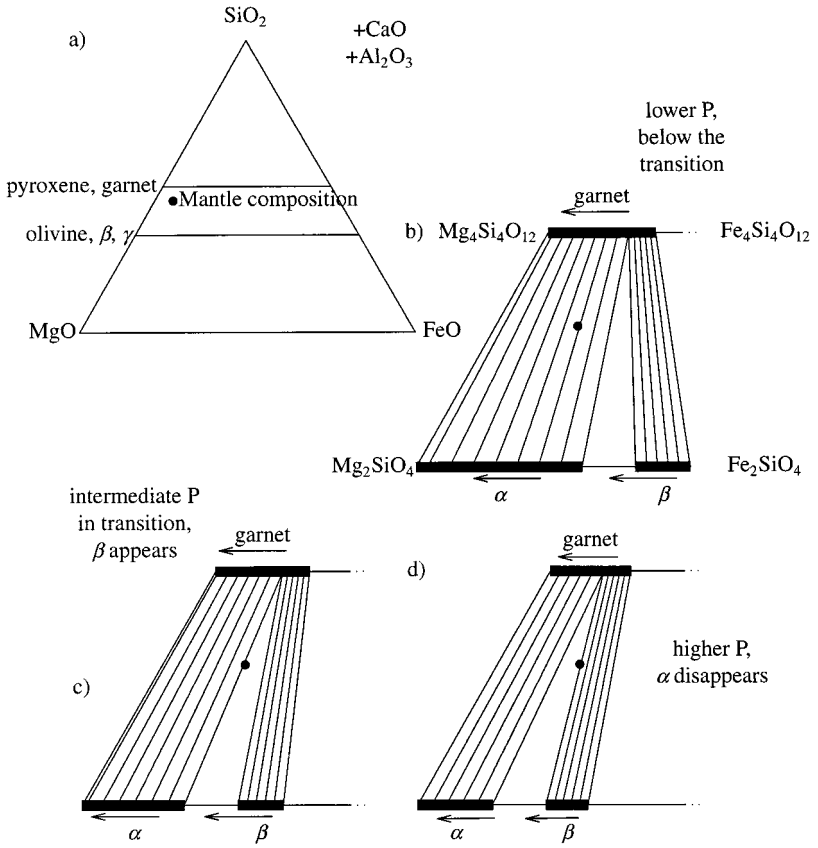

Figure 5. (a) Fe-Mg-Si compositional diagram (projected from Ca and Al) showing positions of major mantle mineral solid solutions olivine, pyroxene, and garnet along lines toward center of triangular region. The dot indicates the mantle's pyrolitic bulk composition, which the mineral proportions must sum to. Remaining panels show blowups of the region in the vicinity of the mantle composition. (b) Tie lines show coexisting composition of garnet/pyroxene + olivine (α) and garnet/pyroxene + wadsleyite (β). Approaching the 410 from lower pressure, α and β and garnet/pyroxene get increasingly enriched in Mg (arrows). Only α and garnet/pyroxene need be present to make up the mantle's bulk composition, so there is no β. (c) Increasing pressure enriches garnet/pyroxene, α and β in Mg. Now β must appear to make up the mantle composition, since the bulk composition no longer lies on a garnet/pyroxene + α tie line. (d) Finally, α disappears at even higher pressure when garnet/pyroxene + β tie line crosses bulk composition. The pressure interval between β debut and α exit might be narrower than depicted in Figure 4 because garnet/pyroxene is not present in the pure olivine system. This could lead to a truncated region of two phase coexistence and a sharp discontinuity.

explain intermittency, for which there is no independent evidence.

In the 660's case the experimentally determined partitioning of Fe and Mg between magnesiowustite and perovskite suggests that the mantle's bulk composition lies very close to the tie lines connecting ringwoodite with its products (reaction (R3)), drastically shortening the transition interval and leading to a seismically sharp discontinuity [*Wood and Rubie*, 1996]. As perovskite absorbs Al from the decomposing majoritic garnet, it also becomes richer in Fe, while magnesiowustite becomes more impoverished. This reaction happens over a broader pressure interval, slowly shifting perovskite and magnesiowustite compositions to collinearity with the mantle's bulk composition. The result is a sharp discontinuity onset superimposed on a gradient zone, which is what Figure 1 shows of the velocity structure in the 660's vicinity.

4.3. Observed 410 Uplift in Subduction Zones

The obvious place to look for discontinuity displacement is in subduction zones on account of their extreme temperature difference relative to the mantle. Thermal modeling is relatively free of uncertainty if we are only seeking a maximum temperature difference between the coldest part of the slab's interior and the mantle [*McKenzie*, 1969]. Thus a check would be to see whether the thermodynamically prescribed deflection of the 410 is compatible with the estimated temperature.

Collier and Helffrich [1997] explored 410 uplift in the Izu-Bonin subduction zone using short-period underside reflections from the 410. They found 410 uplift to ap-

proximately 350 km. Using a seismic Clapeyron slope of 3.1 MPa K^{-1} (Table 1) and an upper mantle 100/3 MPa pressure increase with each kilometer deeper, this corresponds to a ~650-K temperature difference. The minimum slab temperature at 350 km is 760 ± 40 K cooler than the mantle [*Molnar et al*., 1979; *Helffrich and Brodholt*, 1991] (the uncertainty expresses only the lithosphere's possible age range), in reasonable agreement with the combined thermodynamic and seismological estimate.

4.4. Observed 660 Depression in Subduction Zones

Reaction (3)'s negative Clapeyron slope requires that it move to higher pressures at lower temperatures, and again subduction zones are a suitable proving ground. In Izu-Bonin the 660 deepens to ~690 km [*Castle and Creager*, 1997; *Collier and Helffrich*, 1997], leading to temperatures ~700 K cooler using a Clapeyron slope of −2.0 MPa K^{-1} [*Bina and Helffrich*, 1994; *Irifune et al*., 1998]. In this case, similar thermal modeling gives 730 ± 50 K cooler temperatures in the slab relative to ambient mantle at 660 km, agreeing with the combined thermodynamic and seismological estimates.

4.5. The 520 Visibility

Owing to its broader transition interval (Figure 4), the 520 should be seismically less visible because it poorly approximates a discontinuous change in seismic properties. It is not featured in radial velocity models such as the one shown in Figure 1 because an accurate description of short-period seismic wave arrival times does not require its presence. Short-period characterization of the 520 suggests it is diffuse, variously 10–30 km to 50 km thick, with a 1% or less velocity contrast [*Cummins et al*., 1992; *Jones et al*., 1992; *Bostock*, 1996]. Where the 520 emerges is in long-period studies of underside discontinuity reflections using *SdS* or *PdP* [*Shearer*, 1990, 1991; *Flanagan and Shearer*, 1998]. With a large, ~5.1 MPa K^{-1} seismic Clapeyron slope (Table 1), its position will be the most sensitive among (R1)–(R3) to any background thermal variation in the mantle. Thus one expects 520 depths to be variable, which one global characterization confirms. *Flanagan and Shearer* [1998] report that 520 visibility improves as the number of seismograms contributing to its average depth estimate increases. The estimates also show a much broader standard error distribution, unlike 410 and 660's. This suggests greater intrinsic variability in 520 depths, consistent with a broad transition with a larger seismic Clapeyron slope than (R1) or (R3).

4.6. Synthesis

Is it possible to reconcile the evidence against the phase transition origin for the transition zone seismic discontinuities? One problematic aspect is that they do not appear to respond to mantle thermal perturbations as expected, with the 410 rising as the 660 deepens and vice versa. This test is valid only where whatever locally changes the mantle temperature extends through both the 410 and 660. This condition is strictly true only in subduction zones where the dip is vertical, a rare occurrence in the present-day Earth and not satisfied in any area studied to date. Figure 6 shows a set of observations taken from the literature using long-period reflections of nearly vertically traveling shear waves. The discontinuity depths near subduction zones are mostly negatively correlated, showing that when a similar methodology is used in a similar environment, the discontinuities behave as expected.

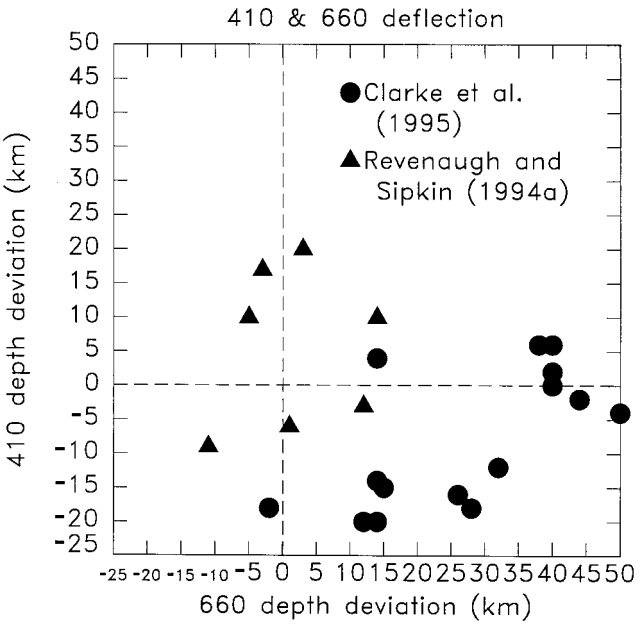

Figure 6. Estimates of 410 and 660 depths using long-period *ScS* reflections taken from the literature [*Revenaugh and Sipkin*, 1994a; *Clarke et al*., 1995]. Revenaugh and Sipkin data are for the subset interacting with the Izu-Bonin subduction zone, and Clarke et al. data are for the South American subduction zone. The quadrants at lower right and upper left contain most of the discontinuity covariation, showing that the discontinuity displacement is anticorrelated.

The other problematic aspect for a phase transition explanation is the amount of topography on the 410, 520, and 660. The 410 and 520's depth variability is lower than the 660's but the seismic Clapeyron slopes for (R1) and (R2) are each larger than for (R3). Resolving this problem requires examining how one obtains global 410 and 520 depth estimates. Small-scale topographic excursions probably are biased toward lower variability on account of the Fresnel zone properties of the long-period underside discontinuity reflections of *PdP* and *SdS*. These arrivals, used for global studies, have large, *sea purse* shaped Fresnel zones that sample very far from their geometric bounce points [*Shearer*, 1991]. On account of *PdP* and *SdS*'s *maximum time* nature, reflections from structures distant from the geometric bounce point arrive earlier than the main arrival, which could be interpreted as a structure under the bounce point,

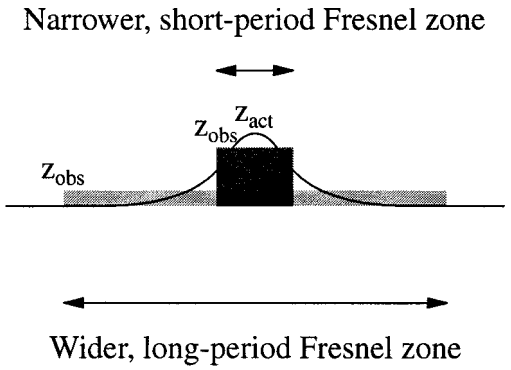

Figure 7. Spatial averaging over narrow structures reduces estimated displacement. If z_{act} is the real discontinuity depth but estimated as z_{obs} by an underside reflection that spatially averages over its Fresnel zone like *PdP*, *SdS*, *pdP*, or *sdP*, the inferred uplift or depression will be too small. Interrogation with shorter-period waves provides less biased depth estimates.

whereas it actually exists elsewhere [*King et al*., 1975; *Weber and Wicks*, 1996; *Schimmel*, 1997]. There is also a fundamental asymmetry between the way underside reflections respond to uplift versus depression of the discontinuity [*Chaljub and Tarantola*, 1997; *Neele et al*., 1997]. While topography is underestimated in simulated geometries for both uplift and depression, uplift on the 410 is underestimated by a factor of 10, whereas 660 depression is underestimated by a factor of 8. Both types of reflections yield discontinuity depth estimates with the wrong sign depending on the bounce point position relative to the topographic extremum, more widely in the case of 410 uplift [*Neele et al*., 1997]. Spatially averaging these estimates would therefore yield smaller topographic uplift on the 410 than the Earth might contain while more faithfully retaining 660 depression features. For the largest conceivable thermal variations in the upper mantle, subducted lithospheric slabs, 410 and 520 uplift would be subdued while 660 depression would be evident. This is the result from studies using longer-period underside reflections [*Shearer*, 1991, 1993; *Flanagan and Shearer*, 1998]. Studies probing discontinuity depth variations in the same areas at shorter periods uniformly show larger topography on the discontinuities than longer-period studies [*Wicks and Richards*, 1993; *Niu and Kawakatsu*, 1995; *Shen et al*., 1996; *Collier and Helffrich*, 1997; *Castle and Creager*, 1997, 1998]. The nature of the biases in global *PdP* and *SdS* studies is still a contentious issue [*Shearer et al*., 1999].

Finally, different methodologies yield different estimates of discontinuity depths, each probably with different biases, succinctly summarized by *Bock et al*. [1995, p. 40]: "... the fact that conflicting results were obtained employing different processing methods is, of course, unsatisfactory." A pragmatic method to assess any study's resolution is to ask what period range of seismic waves constitute the probe. Short-period waves have smaller Fresnel zones and thus average over narrower spatial regions, leading to better resolution of narrow bumps or troughs. This is one reason why short-period topography estimates can be larger than longer-period ones (Figure 7). In one study using waves with a period of 10 s, *van der Lee et al*. [1994] showed that spatial averaging over 150 km of ±15 km zero mean topography made the topographic variation undetectable. Since the largest conceivable temperature variations in the mantle, subducted lithospheric slabs, are ~100 km wide, the full spectrum of topographic variation will be inaccessible to broadly averaging probes.

The transition zone discontinuities observationally behave as the mineralogical transformations (R1) and (R3) should. They change position as prescribed by their thermodynamically refined Clapeyron slopes in the cooler temperatures of subduction zones, both in sign and in magnitude. They can be made seismically sharp either by solid solution modeling or by compositional frustration of a broader phase transformation, both leading to narrow transformation intervals. The property in conflict with their predicted thermodynamic behavior is the magnitude and possibly the sign of the response with respect to temperature, which depends on questionable assumptions about the Earth and the use of a potentially biased probe. In balance, the evidence favors treating the discontinuities as chemical reaction tracers.

5. METHODS AND LIMITATIONS

One way to classify the methods for analyzing transition zone discontinuities is through the constraints that the interaction geometry places on the analysis points. Near-source interactions like *pdP*, *sdP*, and *SdP* only illuminate discontinuities where earthquakes occur, which are predominantly plate boundary regions. In the remaining parts of the Earth, unfortunately extensive, the discontinuity structure will be unknowable. Near-receiver interactions like *Pds* similarly restrict study to areas having seismic stations. Using midpath interactions like *SdS* and *PdP* exposes much of the Earth to study. While restricted to sources mostly near plate boundaries and receivers mostly on continents, the midpoints of the ray path lie in many different types of environments. Studies using midpath interactions generally provide global coverage, tesselating the world into bins and averaging properties in each.

The great strength of underside *PP* and *SS* reflection studies lies in their ability to characterize large-scale discontinuity structure, for example, the difference between continents and ocean basins. *Chaljub and Tarantola* [1997] show that 660 uplift is faithfully estimated at length scales >1500 km and that 660 depression is estimated at length scales >3000 km. Thus, for estimating discontinuity depths worldwide or in broad regions, *PP* and *SS* precursors are ideal on account of the broad coverage they afford and their spatial averaging charac-

teristics [*Shearer*, 1991; *Gössler and Kind*, 1996; *Flanagan and Shearer*, 1998; *Gu et al*., 1998].

Another constraint on discontinuity investigations originates in the characteristics of the seismic source used, which limits the frequency at which the discontinuity may be explored. The time lag between the direct *P* wave and a near-source transition zone discontinuity reflection is up to 40 s for *pdP* and 60 s for *sdP* and *SdP*. This lag is comparable to a cycle of long-period seismic waves, rendering it difficult to separate the discontinuity interaction from the direct arrival. Investigating near-source discontinuities is therefore best done with short-period seismic waves. Use of short-period waves puts further constraints on investigative methods because the signals from discontinuity interactions are generally weaker than the noise levels at seismic stations. Using arrays of seismic stations suppresses the noise and makes the interactions detectable but limits the visible regions to those in range of arrays.

Finally, virtually all present-day discontinuity studies work with the arrival time difference between a discontinuity interaction and some *reference arrival* (compare, for example, *Solomon and U* [1975] and *Roecker* [1985]). This method eliminates significant sources of uncertainty, the earthquake location and origin time, which get subtracted out by working with the time difference. Moreover, if the reference arrival follows nearly the same path through the mantle as the discontinuity interaction (as would *P* for *pdP* or *sdP* in Figure 2, for example), then any unusual structure elsewhere in the mantle and near the seismic station will also be subtracted out. The better the study meets these criteria, the better is its immunity to unknown sources of error.

6. USES

Reactions (R1)–(R3) provide two seismic observables: an arrival time that expresses the discontinuity depth and an amplitude that yields a combination of velocity contrast, density contrast, and transition interval thickness. Each property is a thermodynamic consequence. The first depends on the Clapeyron slope and thus on mantle temperature. The second depends on a broader range of parameters including temperature, solid solution properties, chemical composition, and volume. The focus of the remainder of this review is on surveying past and prospective uses of discontinuity topography and on identifying outstanding problems for future resolution.

6.1. Temperature Change Probe

This application derives directly from (1). Discontinuity depth variations yield mantle temperature estimates by the deviation from the fiducial depth. Various loci in the mantle have been explored this way, by studying 410 and 520 uplift and 660 depression. *Shearer* [1990] used transition zone discontinuity reflection precursors to *SS* and *PP* (*S*410*S*, *S*660*S*, *P*410*P*, *P*660*P*) to investigate global 410- and 660-km discontinuity depths. This study provided the discontinuity depth estimates of 410, 520, and 660 km that now name them (though the estimates reportedly first appeared in a dissertation [*Revenaugh*, 1989]). In further work, *Shearer* [1991, 1993], *Shearer and Masters* [1992], *Gössler and Kind* [1996], *Flanagan and Shearer* [1998] and *Gu et al*. [1998] examined 410, 520, and 660 depths and regional variations in them. *Gössler and Kind* [1996] explored differences in the transition zone's temperature structure beneath continents and oceans, finding the mantle transition zone 5 km thicker under cratonic areas as compared with 9 km thinner under oceans, which translates to ~ -40°C and $\sim +70$°C different temperatures relative to nominal discontinuity depths.

Absolute discontinuity depth estimates are not easy to obtain in these studies because they strongly depend on corrections to *PP* or *SS* times for upper mantle structure at the bounce point [*Shearer*, 1993; *Gössler and Kind*, 1996; *Flanagan and Shearer*, 1998]. The most reliably estimated quantity is the transition zone thickness given by the difference (*S*660*S*-*SS*) − (*S*410*S*-*SS*) or (*P*660*P*-*PP*) − (*P*410*P*-*PP*). Under the probably inappropriate assumption that the discontinuity deflection is due to vertically coherent temperature changes, one translates a transition zone thickness difference into a temperature variation by way of

$$z_{660} - z_{410} = z_{0,660} - z_{0,410} + \delta t \times \frac{dz}{dP} \times \left[\left(\frac{dP}{dT} \right)_{(R3)} - \left(\frac{dP}{dT} \right)_{(R1)} \right]$$

$$\delta z = 250 + \delta t \times \frac{dz}{dP} \times \left[\left(\frac{dP}{dT} \right)_{(R3)} - \left(\frac{dP}{dT} \right)_{(R1)} \right],$$

as were the discontinuity variations reported above. If the deflection is one-sided, yet treated as symmetric, δt will be too low (Figure 8). The results from near-source *sdP* and near-receiver *Pds* studies (to be discussed below) indicate lopsided discontinuity deflections, making these thermal variability estimates lower bounds.

The 660 depression studies include *Barley et al*. [1982], *Bock and Ha* [1984], *Richards and Wicks* [1990], *Vidale and Benz* [1992], *Wicks and Richards* [1993], *Niu and Kawakatsu* [1995], *Castle and Creager* [1997], and *Collier and Helffrich* [1997], all using subduction zone earthquakes to look downward at the underlying discontinuities with either *S*660*P*, *S*410*P*, or both (Figure 2 and Figure 3b). The principal uncertainties in these studies are the earthquake depths themselves (with up to ±10 km depth uncertainty), the typical assumption that the discontinuity is horizontal (which affects the interaction geometry), and the velocity structure near the slab (which distorts ray paths and modifies travel times near the interaction point). A representative error bud-

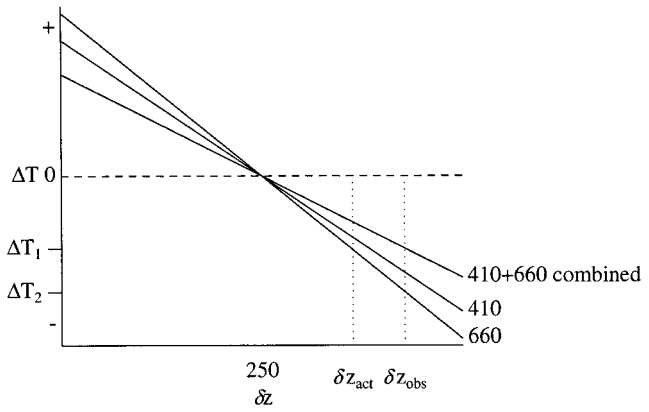

Figure 8. Sources of bias in estimated temperatures in the transition zone. Observed transition zone width z_{obs} yields temperature ΔT_1 if due to combined uplift of 410 and depression of 660. If due only to 660 depression, actual temperature perturbation ΔT_2 is larger. Lopsided discontinuity displacements uniformly yield underestimated transition zone temperatures. A similar argument applies to 410 displacement without any on the 660. Spatial averaging over narrow structures reduces estimated displacement (Figure 7), also leading to the inferred temperature perturbations being too small.

get from these sources is $\sim\pm 11$ km [*Collier and Helffrich*, 1997]. Averaging the mass of individual interaction points over the Fresnel zone leads to shallower depth estimates from a depressed, concave upward discontinuity and deeper estimates from an uplifted, concave downward one, probably by 1–2 km. Despite these biases, most of which lead to shallower discontinuity estimates, the 660 appears to be significantly depressed near subduction zones by 20–30 km (various locations [*Vidale and Benz*, 1992]), 40 km [*Wicks and Richards*, 1993], 30 km [*Castle and Creager*, 1997], and 30 km [*Collier and Helffrich*, 1997] in Izu-Bonin and by 70 km in Tonga [*Bock and Ha*, 1984; *Niu and Kawakatsu*, 1995]. This size deflection suggests 400°–700°C cooler temperatures in slabs relative to the mantle at 660 km depth, except for the extreme values in Tonga, which suggest 1200°C. Rapid subduction of an old slab probably is the reason for this extreme depression [*Okal and Kirby*, 1998].

Similarly, studies using the upgoing near-source reflection from the 410 all indicate 410 uplift in the vicinity of subduction zones between 20 and 60 km [*Vidale and Benz*, 1992; *Zhang and Lay*, 1993; *Collier and Helffrich*, 1997]. *Collier and Helffrich*'s [1997] study investigated the 410's topography close to the active seismicity in the slab and found a 60-km shallower 410 in Izu-Bonin, suggesting ~650°C cooler temperatures there. Intriguingly, in a study of *p*410*P* and *S*410*P* along the western subduction margin of South America, *Collier* [1999] found no 410 deflection in the region where seismicity is absent between ~200 and 600 km. One interpretation of the undeflected 410 is that past subduction of a ridge means the slab is warm at intermediate depths.

6.2. Compositional Changes

Another use for near-source conversions from the 660-km discontinuity (*S*660*P*) is to apply them to the enduring question of whether this discontinuity demarks or accompanies a compositional change. *Castle and Creager* [1997] tested the compositional change idea by looking for the expected deflection of the 660 in subduction zones if it represents the boundary between compositionally different material. They found no detectable *SdP* conversions from elastically different material between 700 and 1000 km depth, concluding that any boundary must either be broad, or closely parallel the 660 in subduction zones, or have a shear velocity contrast less than 1%.

Wood [1995] modeled the effect of water and other contaminants on the position and visibility of the 410. Experiments on wadsleyite show it is able to harbor some trace elements and particularly water more readily than olivine [*Sawamoto and Horiuchi*, 1990; *Gudfinnsson and Wood*, 1998], which tends to stabilize wadsleyite at lower pressures by increasing its entropy, changing the 410's depth. Another effect expected from a component that partitions into wadsleyite rather than olivine is a broadening of the transition interval, making the 410 less reflective to short-period seismic waves. Thus correlated 410 depth and thickness changes could potentially be a prospecting tool for changes in mantle chemistry [*Helffrich and Wood*, 1996]. For all components other than H_2O, both effects appear to be subtle: a maximum of about 2-km broadening and 2-km uplift [*Gudfinnsson and Wood*, 1998]. Given the ± 11 km positional errors on the discontinuities, reliably detecting uplift is problematic. Coupled uplift and broadening could be a more promising approach, but separating true uplift from the downward biased apparent depth poses a difficult measurement challenge.

H_2O's effects on discontinuity properties are more dramatic on account of its strong preference for wadsleyite. If significant water were in the mantle, the 410's breadth would render it undetectable at short periods, placing an upper bound on water abundance in the mantle of about 200 ppm by weight [*Wood*, 1995]. This model could be verified in the vicinity of subduction zones where water is a crucial component in the mantle, promoting melting [*Gill*, 1981]. Moreover, water is thought to contribute to changes in transition zone structure seen at long periods using vertically travelling shear waves (*ScS*) [*Revenaugh and Sipkin*, 1994a, b] by inducing melting in the transition zone. H_2O-rich melt in contact with wadsleyite at the top of the 410 should not only make the discontinuity less visible, but should also raise it. Investigations to date indicate that the 410 in the Izu-Bonin subduction zone is at its fiducial depth but slightly less visible than anticipated [*Collier and Helffrich*, 1997; *Collier*, 1999], suggesting water is not present in significantly greater quantities in deep subduction zone reaches than elsewhere in the mantle.

6.3. Mantle Convective Style

The combination of reaction (3)'s negative Clapeyron slope coupled with the density increase suggests that the discontinuity might impede slab penetration into the lower mantle [*Christensen and Yuen*, 1984]. Over the Earth's age, convective isolation of the upper and lower mantle could lead to compositional differences between them. One way to test whether the mantle convects as a whole is to see whether downward 660 deflections correlate with the buoyancy loads imposed by the overlying upper mantle. Cool, negatively buoyant material in the upper mantle supported by the lower mantle should yield large 660 deflections and consequently lend more credence to the notion of layered mantle convection. *Morgan and Shearer* [1993] found that the 660's topography was too small to support the inferred buoyancy loads, thus favoring whole-mantle convection. Using *SdS*, 660 topography is possibly underestimated, but since the buoyancy loads depend on very broad spatial averages, there probably are not the regional ±30- to 60-km discontinuity depth variations required for layered mantle convection.

6.4. Deep Earthquake Models

One solution to the enigma of deep earthquakes [*Frohlich*, 1989; *Lomnitz-Adler*, 1990] invokes effects related to phase changes in metastable olivine held too cool in the interior of a subducted lithospheric slab to transform to wadsleyite [*Kirby et al*., 1996; *Bina*, 1996]. The simplest model envisages a wedge of metastable olivine bounded by an isotherm extending downward in the slab's core from reaction (1)'s equilibrium position. Since there is no wadsleyite in the slab in the metastable wedge, there should be no visible 410 reflection in the slab. *Collier and Helffrich*'s [1997] study in the Izu-Bonin subduction zone shows the 410 to extend up to 350 km, ruling out the presence of an isotherm-bounded metastable wedge. The 410 elevation in slabs indicates that regions substantially transformed to wadsleyite exist there, so if metastability plays a role, it must do so in a virtually olivine-free milieu.

6.5. Near-Receiver Stacking

A testimonial to the versatility of near-receiver discontinuity conversion studies using *P*660*s* and *P*410*s* is their varied uses. *Paulssen* [1988] investigated discontinuity sharpness by seeking 410 and 660 conversions under Europe and North America, reporting a less visible 410 as compared with the 660 on the basis of fewer observed discrete arrivals. Similarly, *van der Lee et al*. [1994] investigated the transition zone under the Netherlands and found that small-scale 660 topography, varying ±15–25 km in height and 100–200 km laterally, explained the complete absence of *Ps* discontinuity conversions in the individual seismograms collected in this region. In contrast, *Gurrola et al*. [1994] processed a collection of records simultaneously to estimate the 660 discontinuity depth under a continental Asian station, finding it visible at a most likely depth of 663 km. *Bostock* [1996] and *Li et al*. [1998] also used *Pds* in continental areas to examine the thermal structure below cratonic roots to see whether they extend into the transition zone. *Dueker and Sheehan* [1998] similarly investigated the transition zone beneath the Colorado Plateau. In tectonically younger areas, *Shen et al*. [1996, 1998] prospected for thermal effects in the transition zone related to the mantle plume associated with the Iceland hotspot, as did *Dueker and Sheehan* [1997] under the Snake River Plain near the Yellowstone hotspot. In subduction zones, *Thirot et al*. [1998] used near-receiver conversions from both the 410 and 660 to examine the influence of subducted slabs on the discontinuities.

In order to convert the times obtained from *Ps* conversion observations to discontinuity depths, one needs an accurate velocity model for the path between the conversion point and the receiver, akin to the methods used to interpret the *SdS* observations discussed earlier. The depths these studies provide thus should be viewed as conditional on the velocity model used for correcting the lag times [*Stammler et al*., 1992; *Gurrola et al*., 1994; *Chevrot et al*., 1999]. As with *SdS*, one can avoid much of the bias associated with the use of an unsuitable transition zone velocity model by interpreting *P*660*s*–*P*410*s* times rather than *P*660*s*-*P* and *P*410*s*-*P*, with a consequent loss of absolute depth information. *Li et al*. [1998] investigated the eastern North American transition zone, seeking evidence for convection associated with the possibly cool cratonic root bordering the region. Using *P*660*s*–*P*410*s* times, these authors reported significant changes in the transition zone thickness not correlated with the cratonic root's position. Using *Grand*'s [1994] model to obtain absolute depths, some startling results emerged. The authors found the 410 depth uniform throughout the region yet the 660 alternately depressed by ~20 km and raised by ~10 km in different regions of the study area.

Dueker and Sheehan [1998] found regional variations in the transition zone thickness below the Rocky Mountains and the Colorado Plateau of ~30 km. The distribution of thickness spot estimates is curiously bimodal, peaking at 260 and 290 km. Correcting the *Ps* times with *Lee and Grand*'s [1996] tomographic model, they found ±10 km variations in 410 depth around an average of 419 km, and ±20 km variations in 660 depth around a 677 km depth average. The results from both of these continental studies underscore the questionable nature of the assumption of vertically coherent temperature changes in the mantle as well as the possibility of one-sided discontinuity displacement when interpreting transition zone thicknesses.

Similarly, *Shen et al*. [1996, 1998] examined the transition zone under the Iceland hotspot for any thermal effects due to the presence of an underlying mantle plume, correcting travel times with results from a regional tomographic study [*Wolfe et al*., 1997]. They found a 23-km-thinner transition zone here, corresponding to

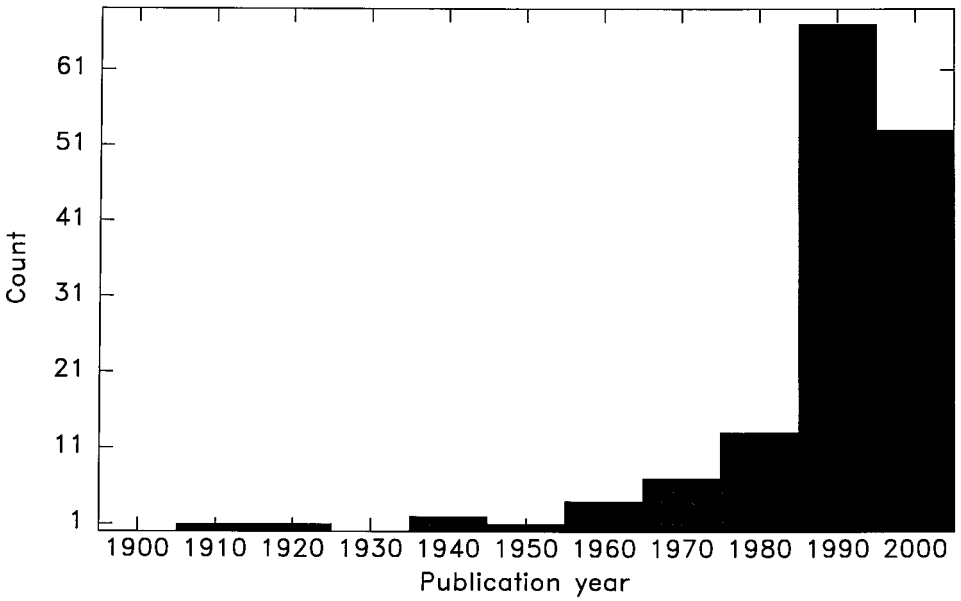

Figure 9. Number of papers published per year relating to discontinuities.

temperatures along an adiabat 180°C warmer than normal mantle through the transition zone, and with 660 uplift toward the south of the island. The dominant influence in the raw 410 and 660 lag times is the transition zone structure above the 410 because the times correlate positively rather than negatively. The differential *P*660*s*–*P*410*s* times reveal the thinning.

7. OUTLOOK

Transition zone discontinuity studies appear to be mature probes of transition zone temperature structure, contributing to the general understanding of the dynamics of the transition zone. They have yet to make their mark as probes of lateral chemical changes in the mantle, for two reasons. First, a convincing demonstration of their ability to detect chemical changes is yet to be shown. Second, the seismological observable is a change in converted wave amplitude. At interesting scales in the mantle, the ~100 km thickness of lithospheric slabs [*Stein and Stein*, 1992] and the ~200 km width of mantle plumes [*Sleep*, 1992], one needs short-period waves to resolve the structures. Unfortunately, short-period waves are generally noisy, masking the low-amplitude discontinuity arrivals. We might anticipate advances in processing techniques to provide new methods if the past is any guide (Figure 9). Applying scattering methods to probe sub-Fresnel-zone-sized structures [*Doornbos*, 1992; *Cormier*, 1995; *Ji and Nataf*, 1998; *Hedlin et al*., 1997; *Kaneshima and Helffrich*, 1998; *Castle and Creager*, 1999] is one developmental front which may open the discipline to global study using longer-period waves.

Finally, portable broadband seismometer deployments above interesting mantle dynamical targets will increase with time [*Incorporated Research Institutions for Seismology*, 1995]. These deployments have previously been used at ~100-km station spacing, but the noise reduction and spatial coverage provided by denser array spacing will provide new insights into mantle dynamics, much like smaller arrays did when introduced in the 1960s, leading to the first insights into the nature of the transition zone's discontinuities [*Engdahl and Flinn*, 1969; *Whitcomb and Anderson*, 1970; *Richards*, 1972; *Teng and Tung*, 1973; *King et al*., 1975].

GLOSSARY

410, 520, 660: These are names given to the seismic discontinuities nominally at those kilometer depths in the average mantle (Figure 1). Changes in mantle temperature or composition may raise or lower their position, so the name is generic rather than indicating a precise depth. Over time, average seismic velocity models of the Earth improve, as do the average depths of these discontinuities. The 410 and 660 previously were known as the "400" and the "670"; the 520 has not had a previous alias.

Fresnel zone: Though idealized as rays as in Figure 1, seismic waves propagate through some finite volume of the Earth. Longer wavelengths naturally involve more of the Earth. A useful way to isolate the part of the Earth that contributes to a seismic wave arrival is in terms of the Fresnel zone. This is the set of points that the wave might travel to from the source, interact with, and return to the receiver within a quarter period of the fastest possible path. Any part of the Earth in this point set palpably affects the seismic wave's arrival. See Figure 3 for some Fresnel zone illustrations.

Long-period, short period: The Earth vibrates in many different frequency ranges. Waves whose periods are 10,000–200 s include the free oscillations of the Earth and surface waves. Body waves, which follow ray-like paths through the volume of the Earth, are termed long period when they have 200- to 10-s periods and are termed short period if they are, of course, shorter. Attenuative damping of short-period body waves that travel substantial distances ($>10^3$ km) through the Earth limits the highest usable frequency to about 10 Hz.

Minimum, maximum time: Distinct phases correspond to a zero first derivative of the seismic wave travel time with respect to a spatial parameter, such as a bounce-point position from the Earth's surface. A local travel time minimum or a local travel time maximum might cause the zero. If a local minimum, nothing else arrives earlier; *pP* and *sP* are both minimum time phases. For a local maximum, everything else arrives earlier but acts to cancel out the effects of all but the latest-arriving energy. Any heterogeneity in the earlier arrivals leads to imperfect cancelation and affects the shape and timing of the maximum time phase. *SS* and *PP* are such phases.

Period: The reciprocal of a wave's frequency. This represents the time it takes a sinusoidal wave passing some point to return to its initial conditions. Given a wave speed, the shorter the period, the shorter the wavelength. See wavelength, frequency, and speed, below.

Phase: A confusing term with different meanings in seismology and thermodynamics. A distinct arrival in the wave field emanating from the seismic source is called a phase by a seismologist. On the other hand, a thermodynamicist calls a part of a system with uniform and distinct mechanical properties a phase, too. *P* and *S* waves are different phases in the wave field, and olivine and ringwoodite are different phases of Mg_2SiO_4. Hopefully, context distinguishes the meanings.

Phase transition: Another name for a chemical reaction between reactants and products. The reaction might be homogeneous (reactant A = product B), like the olivine to wadsleyite transition (reaction (R1)), or heterogeneous (reactant A + reactant B = product C + product D), like the ringwoodite to magnesiowustite + perovskite (reaction (R3)) transition.

Precursor: A minor (low amplitude) seismic wave arrival preceding a major one (higher amplitude). One source of these is a discontinuity reflection.

Reference arrival: A major seismic wave arrival (see phase) that establishes a point in time within the propagating wave field to compare to other arrival times. Seismologists use these to establish a relative time base free from some major sources of observational uncertainty. Two of these are improperly set clocks at seismic stations and incompletely known earthquake locations in space and time. If the reference phase's path through the Earth is similar to the arrival being studied, it also feels the same along-path influences of any unusual Earth structure. Using the difference in arrival times between the reference phase and the phase under study removes the adverse effects due to unexpected Earth structure.

Reflection, refraction: These are the primary means for detecting a seismic discontinuity. When a wave interacts with a steep gradient region or a discontinuity in elastic properties, part of its energy is reflected away from the region, while the balance goes through it. Refraction describes this transmission.

Sea purse: A sea purse is the bladder-shaped egg case of an elasmobranch fish like a shark or dogfish, often found washed up on the beach. Translucent pale-brown in color while fresh, they harden and dry to iodine brown. They have the appearance of a lozenge with elongate, tentacle-shaped corners.

Source, receiver: Being indifferent to the nature of the process that generates a seismic wave for them to study, seismologists generically term the process a source. It might be an explosion, an earthquake, a mine collapse, a meteorite impact, or a sonic boom. Receivers, on the other hand, are the seismometers that detect the incoming seismic waves.

Transition zone: *Birch* [1952] gave this name to the region of the upper mantle where the increases in seismic wave speed with depth did not appear to be due solely to self-compression of the body of the Earth. He recognized the region to be a zone of transition between seismic wave speed increases brought about by some unknown mechanism and the better understood one of self-compression, christening the region in an impartial way. The transition zone's limits are defined via seismic wave speed gradient anomalies. Over time, these change due to the continual refinements in the Earth's seismic wave speed profiles. Consequently, reading older literature in search of precise transition zone bounds is a frustrating exercise.

Wavelength, frequency, speed: These are mutually interdependent, through the formula for the speed $v = f\lambda$. At some frequency f, wavelengths λ in slower materials are longer and conversely are shorter for faster materials. Thus *P* waves are longer wavelength than *S* waves at the same frequency.

ACKNOWLEDGMENTS. You would have read a much less precise and more opaque contribution had Justin Revenaugh not spent time unselfishly editing the original text. I am also grateful for Pierre Vacher's and Yohsuke Kamide's reviews, which provided valuable suggestions and reminded me of the clarity required to engage the international readership. Mike Kendall's insights into the manuscript's structure helped maintain a semblance of balance in the argument as well. Bernie Wood contributed the valuable perspective of the "non-geophysicist with a need to know" by suggesting improvements to many of the figures and the text. Cheril Cheverton, Jon Collier, and Dave Gubbins also provided sensible criticisms of previous drafts.

Roel Snieder was the Editor responsible for this paper. He

thanks Pierre Vacher and Justin Revenaugh for the technical reviews and Yoshuke Kamide for the cross-disciplinary review.

REFERENCES

Adams, R. D., Reflections from discontinuities beneath Antarctica, *Bull. Seismol. Soc. Am*., *61*, 1441–1451, 1971.

Akaogi, M., E. Ito, and A. Navrotsky, Olivine-modified spinel-spinel transitions in the system Mg_2SiO_4–Fe_2SiO_4: Calorimetric measurements, thermochemical calculation, and geophysical application, *J. Geophys. Res*., *94*, 15,671–15,685, 1989.

Barley, B. J., J. A. Hudson, and A. Douglas, *S* to *P* scattering at the 650 km discontinuity, *Geophys. J. R. Astron. Soc*., *49*, 773–777, 1982.

Bass, J. D., and D. L. Anderson, Composition of the upper mantle: Geophysical tests of two petrological models, *Geophys. Res. Lett*., *11*, 229–232, 1984.

Bass, J. D., and D. L. Anderson, Composition of the upper mantle: Geophysical tests of two petrological models, *Geophys. Res. Lett*., *11*, 229–232, 1984.

Benz, H. M., and J. E. Vidale, Sharpness of upper-mantle discontinuities determined from high-frequency reflections, *Nature*, *365*, 147–150, 1993.

Bernal, J. D., Geophysical discussion, *Observatory*, *59*, 265–269, 1936.

Bina, C. R., Phase transition buoyancy contributions to stresses in subducting lithosphere, *Geophys. Res. Lett*., *23*, 3563–3566, 1996.

Bina, C. R., and G. R. Helffrich, Phase transition Clapeyron slopes and transition zone seismic discontinuity topography, *J. Geophys. Res*., *99*, 15,853–15,860, 1994.

Bina, C. R., and B. J. Wood, Olivine-spinel transitions: Experimental and thermodynamic constraints and implications for the nature of the 400-km seismic discontinuity, *J. Geophys. Res*., *92*, 4853–4866, 1987.

Birch, F., Elasticity and constitution of the Earth's interior, *J. Geophys. Res*., *57*, 227–286, 1952.

Birch, F., Composition of the Earth's mantle, *Geophys. J. R. Astron. Soc*., *4*, 295–311, 1961.

Bock, G., and J. Ha, Short-period *S*–*P* conversion in the mantle at a depth near 700 km, *Geophys. J. R. Astron. Soc*., *77*, 593–615, 1984.

Bock, G., J. Gössler, W. Hanka, R. Kind, G. Kosarev, N. Petersen, K. Stammler, and L. Vinnik, On the seismic discontinuities in the upper mantle, *Phys. Earth Planet. Inter*., *92*, 39–43, 1995.

Bostock, M. G., *Ps* conversions from the upper mantle transition zone beneath the Canadian landmass, *J. Geophys. Res*., *101*, 8393–8402, 1996.

Castle, J. C., and K. C. Creager, Seismic evidence against a mantle chemical discontinuity near 660 km depth beneath Izu-Bonin, *Geophys. Res. Lett*., *24*, 241–244, 1997.

Castle, J. C., and K. C. Creager, Topography of the 660-km seismic discontinuity beneath Izu-Bonin: Implications for tectonic history and slab deformation, *J. Geophys. Res*., *103*, 12,511–12,527, 1998.

Castle, J. C., and K. C. Creager, A steeply dipping discontinuity in the lower mantle beneath Izu-Bonin, *J. Geophys. Res*., *104*, 7279–7292, 1999.

Chaljub, E., and A. Tarantola, Sensitivity of *SS* precursors to topography on the upper mantle 660-km discontinuity, *Geophys. Res. Lett*., *24*, 2613–2616, 1997.

Chevrot, S., L. Vinnik, and J.-P. Montagner, Global-scale analysis of the mantle *Pds* phases, *J. Geophys. Res*., *104*, 20,203–20,219, 1999.

Chopelas, A., R. Boehler, and T. Ko, Thermodynamics and behavior of γ-Mg_2SiO_4 at high pressure: Implications for Mg_2SiO_4 phase equilibrium, *Phys. Chem. Miner*., *21*, 351–359, 1994.

Christensen, U., and D. Yuen, The interaction of a subducting lithospheric slab with a chemical or phase boundary, *J. Geophys. Res*., *89*, 4389–4402, 1984.

Clarke, T., P. G. Silver, Y.-L. Yeh, D. E. James, T. C. Wallace, and S. L. Beck, Close in *ScS* and *sScS* reverberations from the June 9, 1994, Bolivian earthquake, *Geophys. Res. Lett*., *22*, 2313–2316, 1995.

Collier, J. D., An investigation of the depths and properties of the mantle's seismic discontinuities in subduction zones, doctoral thesis, Fac. of Sci., Dep. of Earth Sci., Univ. of Bristol, Bristol, England, 1999.

Collier, J., and G. Helffrich, Topography of the "410" and "660" km seismic discontinuities in the Izu-Bonin subduction zone, *Geophys. Res. Lett*., *24*, 1535–1538, 1997.

Cormier, V. F., Time-domain modeling of PKIKP precursors for constraints on the heterogeneity in the lowermost mantle, *Geophys. J. Int*., *121*, 725–736, 1995.

Cummins, P., B. L. N. Kennett, J. R. Bowman, and M. G. Bostock, The 520 km discontinuity?, *Bull. Seismol. Soc. Am*., *82*, 323–336, 1992.

Doornbos, D. J., Diffraction and seismic tomography, *Geophys. J. Int*., *108*, 256–266, 1992.

Dueker, K., and A. Sheehan, Mantle discontinuity structure from midpoint stacks of converted *P* and *S* waves across the Yellowstone hotspot track, *J. Geophys. Res*., *102*, 8313–8327, 1997.

Dueker, K., and A. Sheehan, Mantle discontinuity structure beneath the Colorado Rocky Mountains and High Plains, *J. Geophys. Res*., *103*, 7153–7169, 1998.

Engdahl, E. R., and E. A. Flinn, Seismic waves reflected from discontinuities within the Earth's upper mantle, *Science*, *163*, 177–179, 1969.

Fei, Y.-W., and C. Bertka, The α-β transition in systems relevant to the upper mantle (abstract), *Eos Trans. AGU*, *77*(46), Fall Meet. Suppl., F649, 1996.

Ferguson, F. D., and T. K. Jones, *The Phase Rule*, 112 pp., Butterworths, London, 1966.

Flanagan, M. P., and P. M. Shearer, Global mapping of topography on transition zone velocity discontinuities by stacking *SS* precursors, *J. Geophys. Res*., *103*, 2673–2692, 1998.

Frohlich, C., The nature of deep-focus earthquakes, *Annu. Rev. Earth Planet. Sci*., *17*, 227–254, 1989.

Furukawa, Y., Two types of deep seismicity in subducting slabs, *Geophys. Res. Lett*., *21*, 1181–1184, 1994.

Gill, J., *Orogenic Andesites*, 385 pp., Springer-Verlag, New York, 1981.

Gössler, J., and R. Kind, Seismic evidence for very deep roots of continents, *Earth Planet. Sci. Lett*., *138*, 1–13, 1996.

Grand, S. P., Mantle shear structure beneath the Americas and surrounding oceans, *J. Geophys. Res*., *99*, 11,591–11,621, 1994.

Gu, Y., A. M. Dziewonski, and C. B. Agee, Global de-correlation of the topography of transition zone discontinuities, *Earth Planet. Sci. Lett*., *157*, 57–67, 1998.

Gudfinnsson, G. H., and B. J. Wood, The effect of trace elements on the olivine-wadsleyite transformation, *Am. Mineral*., *83*, 1037–1044, 1998.

Gurrola, H., J. B. Minster, and T. Owens, The use of velocity spectrum for stacking receiver functions and imaging upper mantle discontinuities, *Geophys. J. Int*., *117*, 427–440, 1994.

Hedlin, M. A. H., P. M. Shearer, and P. S. Earle, Seismic evidence for small-scale heterogeneity throughout the Earth's mantle, *Nature*, *387*, 145–150, 1997.

Helffrich, G. R., and C. R. Bina, Frequency dependence of the visibility and depths of mantle seismic discontinuities, *Geophys. Res. Lett*., *21*, 2613–2616, 1994.

Helffrich, G., and J. Brodholt, The relationship of deep seismicity to the thermal age of subducted lithosphere, *Nature*, *353*, 252–255, 1991.

Helffrich, G. R., and B. J. Wood, 410 km discontinuity sharpness and the form of the olivine α-β phase diagram: Resolution of apparent seismic contradictions, *Geophys. J. Int.*, *126*, F7–F12, 1996.

Incorporated Research Institutions for Seismology Consortium, A science facility for studying the dynamics of the solid Earth, proposal submitted to the U.S. National Science Foundation, August 1995, Washington, D. C., 1995.

Irifune, T., and M. Isshiki, Iron partitioning in a pyrolite mantle and the nature of the 410-km seismic discontinuity, *Nature*, *392*, 702–705, 1998.

Irifune, T., et al., The postspinel phase boundary in Mg_2SiO_4 determined by in situ X-ray diffraction, *Science*, *279*, 1698–1700, 1998.

Ita, J., and L. Stixrude, Petrology, elasticity, and composition of the mantle transition zone, *J. Geophys. Res.*, *97*, 6849–6866, 1992.

Ito, E., and E. Takahashi, Postspinel transformations in the system Mg_2SiO_4–Fe_2SiO_4 and some geophysical implications, *J. Geophys. Res.*, *94*, 10,637–10,646, 1989.

Jeanloz, R., Effects of phase transitions and possible compositional changes on the seismological structure near 650-km depth, *Geophys. Res. Lett.*, *18*, 1743–1746, 1991.

Jeanloz, R., and A. B. Thompson, Phase transitions and mantle discontinuities, *Rev. Geophys.*, *21*, 51–74, 1983.

Ji, Y., and H.-C. Nataf, Detection of mantle plumes in the lower mantle by diffraction tomography: Theory, *Earth Planet. Sci. Lett.*, *159*, 87–98, 1998.

Jones, L. E., J. Mori, and D. V. Helmberger, Short-period constraints on the proposed transition zone discontinuity, *J. Geophys. Res.*, *97*, 8765–8774, 1992.

Kaneshima, S., and G. Helffrich, Detection of lower mantle scatterers northeast of the Mariana subduction zone using short-period array data, *J. Geophys. Res.*, *103*, 4825–4838, 1998.

Katsura, T., and E. Ito, The system Mg_2SiO_4–Fe_2SiO_4 at high pressures and temperatures: Precise determination of stabilities of olivine, modified spinel, and spinel, *J. Geophys. Res.*, *94*, 15,663–15,670, 1989.

Kennett, B. L. N., E. R. Engdahl, and R. Buland, Constraints on seismic velocities in the Earth from traveltimes, *Geophys. J. Int.*, *122*, 108–124, 1995.

Kincaid, C., and P. Olson, An experimental study of subduction and slab migration, *J. Geophys. Res.*, *92*, 13,832–13,840, 1987.

King, D. W., R. A. W. Haddon, and E. S. Husebye, Precursors to *PP*, *Phys. Earth Planet. Inter.*, *10*, 103–127, 1975.

Kirby, S. H., S. Stein, E. Okal, and D. C. Rubie, Metastable mantle phase transformations and deep earthquakes in subducting oceanic lithosphere, *Rev. Geophys.*, *34*, 261–306, 1996.

Lee, D. K., and S. P. Grand, Upper mantle shear structure beneath the Colorado Rocky Mountains, *J. Geophys. Res.*, *101*, 22,233–22,244, 1996.

Lees, A., M. S. T. Bukowinski, and R. Jeanloz, Reflection properties of phase transition and compositional change models of the 670-km discontinuity, *J. Geophys. Res.*, *88*, 8145–8159, 1983.

Lehmann, I., *P′*, *Union Géod. Géophys. Int., Assoc. Seismol., Ser. A, Trav. Sci.*, *14*, 87–115, 1936.

Li, A., K. M. Fischer, M. E. Wysession, and T. J. Clarke, Mantle discontinuities and temperature under the North American continental keel, *Nature*, *395*, 160–163, 1998.

Lomnitz-Adler, J., Are deep-focus earthquakes caused by a martensitic transformation?, *J. Phys. Earth*, *38*, 83–93, 1990.

McKenzie, D. P., Speculations on the consequences and causes of plate motions, *Geophys. J. R. Astron. Soc.*, *18*, 1–32, 1969.

Meijering, J. L., and C. J. M. Rooymans, On the olivine-spinel transformation in the Earth's mantle, *K. Ned. Akad. Wet.*, *61*, 333–344, 1958.

Molnar, P., D. Freedman, and J. F. Shih, Lengths of intermediate and deep seismic zones and temperatures in downgoing slabs of lithosphere, *Geophys. J. R. Astron. Soc.*, *56*, 41–54, 1979.

Morgan, J. P., and P. M. Shearer, Seismic constraints on mantle flow and topography of the 660-km discontinuity: Evidence for whole-mantle convection, *Nature*, *365*, 506–511, 1993.

Morishima, H., T. Kato, M. Suto, E. Ohtani, S. Urakawa, W. Utsumi, O. Shimomura, and T. Kikegawa, The phase boundary between α- and β-Mg_2SiO_4 determined by in situ X-ray observation, *Science*, *265*, 1202–1203, 1994.

Nakanishi, I., Seismic reflections from the upper mantle discontinuities beneath the Mid-Atlantic Ridge observed by a seismic array in Hokkaido region, Japan, *Geophys. Res. Lett.*, *13*, 1458–1461, 1986.

Nakanishi, I., Reflections of *P′P′* from upper mantle discontinuities beneath the Mid-Atlantic Ridge, *Geophys. J.*, *93*, 335–346, 1988.

Neele, F., H. de Regt, and J. VanDecar, Gross errors in upper-mantle discontinuity topography from underside reflection data, *Geophys. J. Int.*, *129*, 194–204, 1997.

Niu, F., and H. Kawakatsu, Direct evidence for the undulation of the 660-km discontinuity beneath Tonga: Comparison of Japan and California array data, *Geophys. Res. Lett.*, *22*, 531–534, 1995.

Okal, E. A., and S. Kirby, Deep earthquakes beneath the Fiji Basin, SW Pacific: Earth's most intense deep seismicity in stagnant slabs, *Phys. Earth Planet. Inter.*, *109*, 25–63, 1998.

Oldham, R. D., Constitution of the interior of the Earth as revealed by earthquakes, *Q. J. Geol. Soc. London*, *62*, 456–475, 1906.

Paulssen, H., Evidence for a sharp 670-km discontinuity as inferred from *P*-to-*S* converted waves, *J. Geophys. Res.*, *93*, 10,489–10,500, 1988.

Petersen, N., L. Vinnik, G. Kosarev, R. Kind, S. Oreshin, and K. Stammler, Sharpness of the mantle discontinuities, *Geophys. Res. Lett.*, *20*, 859–862, 1993.

Revenaugh, J., *The Nature of Mantle Layering From First-Order Reverberations*, Mass. Inst. of Technol., Cambridge, 1989.

Revenaugh, J., and T. H. Jordan, Mantle layering from *ScS* reverberations, 2, The transition zone, *J. Geophys. Res.*, *96*, 19,763–19,780, 1991.

Revenaugh, J., and S. A. Sipkin, Mantle discontinuity structure beneath China, *J. Geophys. Res.*, *99*, 21,911–21,927, 1994a.

Revenaugh, J., and S. A. Sipkin, Seismic evidence for silicate melt atop the 410-km mantle discontinuity, *Nature*, *369*, 474–476, 1994b.

Richards, M. A., and C. W. Wicks, *S–P* conversion from the transition zone beneath Tonga and the nature of the 670 km discontinuity, *Geophys. J. Int.*, *101*, 1–35, 1990.

Richards, P. G., Seismic waves reflected from velocity gradient anomalies within the Earth's upper mantle, *Z. Geophys.*, *38*, 517–527, 1972.

Rigden, S., G. D. Gwanmesia, J. D. Fitz Gerald, I. Jackson, and R. C. Liebermann, Spinel elasticity and seismic structure of the transition zone of the mantle, *Nature*, *354*, 143–145, 1991.

Ringwood, A. E., The constitution of the mantle, I, Thermodynamics of the olivine-spinel transition, *Geochim. Cosmochim. Acta*, *13*, 303–321, 1958a.

Ringwood, A. E., The constitution of the mantle, II, Further data on the olivine-spinel transition, *Geochim. Cosmochim. Acta*, *15*, 18–29, 1958b.

Ringwood, A. E., *Composition and Petrology of the Earth's Interior*, McGraw-Hill, New York, 1975.

Roecker, S. W., Velocity structure in the Izu-Bonin seismic zone and the depth of the olivine-spinel phase transition in the slab, *J. Geophys. Res*., *90*, 7771–7794, 1985.

Sawamoto, H., and H. Horiuchi, β-$(Mg_{0.9}, Fe_{0.1})_2SiO_4$: Single crystal structure, cation distribution, and properties of coordination polyhedra, *Phys. Chem. Miner*., *17*, 293–300, 1990.

Schimmel, M., Distinct body wave phenomena caused by mantle structure, doctoral thesis, 101 + vii pp., Fac. of Earth Sci., Univ. of Utrecht, Utrecht, Netherlands, 1997.

Shearer, P. M., Seismic imaging of upper-mantle structure with new evidence for a 520-km discontinuity, *Nature*, *344*, 121–126, 1990.

Shearer, P. M., Constraints on upper mantle discontinuities from observations of long-period reflected and converted phases, *J. Geophys. Res*., *96*, 18,147–18,182, 1991.

Shearer, P. M., Global mapping of upper mantle reflectors from long-period *SS* precursors, *Geophys. J. Int*., *115*, 878–904, 1993.

Shearer, P. M., and T. G. Masters, Global mapping of topography on the 660-km discontinuity, *Nature*, *355*, 791–796, 1992.

Shearer, P. M., M. P. Flanagan, and M. A. H. Hedlin, Experiments in migration processing of *SS* precursor data to image upper mantle discontinuity structure, *J. Geophys. Res*., *104*, 7229–7242, 1999.

Shen, Y., S. C. Solomon, I. T. Bjarnason, and G. M. Purdy, Hot mantle transition zone beneath Iceland and the adjacent Mid-Atlantic Ridge inferred from *P*-to-*S* conversions at the 410- and 660-km discontinuities, *Geophys. Res. Lett*., *23*, 3527–3530, 1996.

Shen, Y., S. C. Solomon, I. T. Bjarnason, and C. J. Wolfe, Seismic evidence for a lower mantle origin of the Iceland plume, *Nature*, *395*, 62–65, 1998.

Sleep, N. H., Hotspot volcanism and mantle plumes, *Annu. Rev. Earth Planet. Sci*., *20*, 19–43, 1992.

Sobel, P. A., The phase *P′dP′* as a means of determining upper mantle structure, doctoral thesis, 129 pp., Grad. School, Univ. of Minn., Minneapolis, 1978.

Solomon, S. C., and K. T. P. U, Elevation of the olivine-spinel transition in subducted lithosphere: Seismic evidence, *Phys. Earth Planet. Inter*., *11*, 97–108, 1975.

Song, X., and D. V. Helmberger, Seismic evidence for an inner core transition zone, *Science*, *282*, 924–927, 1998.

Stammler, K., and R. Kind, Comment on "Mantle layering from *ScS* reverberations, 2, The transition zone" by Justin Revenaugh and Thomas H. Jordan, *J. Geophys. Res*., *97*, 17,547–17,548, 1992.

Stammler, K., R. Kind, N. Petersen, G. Kosarev, L. Vinnik, and L. Qiyuan, The upper mantle discontinuities: Correlated or anticorelated?, *Geophys. Res. Lett*., *19*, 1563–1566, 1992.

Stein, C., and S. Stein, A model for the global variation in oceanic depth and heat flow with lithospheric age, *Nature*, *359*, 123–129, 1992.

Stixrude, L., Structure and sharpness of phase transitions and mantle discontinuities, *J. Geophys. Res*., *102*, 14,835–14,852, 1997.

Stixrude, L., R. J. Hemley, Y. Fei, and H. K. Mao, Thermoelasticity of silicate perovskite and magnesiowustite and stratification of the Earth's mantle, *Science*, *257*, 1099–1101, 1992.

Teng, T.-L., and J. P. Tung, Upper-mantle discontinuity from amplitude data of *P′P′* and its precursors, *Bull. Seismol. Soc. Am*., *63*, 587–597, 1973.

Thirot, J.-L., J.-P. Montagner, and L. Vinnik, Upper-mantle seismic discontinuities in a subduction zone (Japan) investigated from *P* to *S* converted waves, *Phys. Earth Planet. Inter*., *108*, 61–80, 1998.

Vacher, P., A. Mocquet, and C. Sotin, Computation of seismic discontinuity profiles from mineral physics: The importance of the non-olivine components for explaining the 660 km depth discontinuity, *Phys. Earth Planet. Inter*., *106*, 275–298, 1998.

van der Lee, S., H. Paulssen, and G. Nolet, Variability of P660s phases as a consequence of topography on the 660 km discontinuity, *Phys. Earth Planet. Inter*., *86*, 147–164, 1994.

Vidale, J. E., and H. M. Benz, Upper-mantle seismic discontinuities and the thermal structure of subduction zones, *Nature*, *356*, 678–683, 1992.

Vidale, J. E., X.-Y. Ding, and S. P. Grand, The 410-km-depth discontinuity: A sharpness estimate from near-critical reflections, *Geophys. Res. Lett*., *22*, 2557–2560, 1995.

Wajeman, N., Detection of underside *P* reflections at mantle discontinuities by stacking broadband data, *Geophys. Res. Lett*., *15*, 669–672, 1988.

Weber, M., and C. W. Wicks Jr., Reflections from a distant subduction zone, *Geophys. Res. Lett*., *23*, 1453–1456, 1996.

Whitcomb, J. H., and D. L. Anderson, Reflection of *P′P′* seismic waves from discontinuities in the mantle, *J. Geophys. Res*., *75*, 5713–5728, 1970.

Wicks, C. W., and M. A. Richards, A detailed map of the 660-kilometer discontinuity beneath the Izu-Bonin subduction zone, *Science*, *261*, 1424–1427, 1993.

Williamson, E. D., and L. H. Adams, Density distribution in the Earth, *J. Wash. Acad. Sci*., *13*, 413–432, 1923.

Wolfe, C. J., I. T. Bjarnason, J. C. VanDecar, and S. C. Solomon, Seismic structure of the Iceland mantle plume, *Nature*, *385*, 245–247, 1997.

Wood, B. J., Postspinel transformations and the width of the 670-km discontinuity: A comment on "Postspinel transformations in the system Mg_2SiO_4–Fe_2SiO_4 and some geophysical implications" by E. Ito and E. Takahashi, *J. Geophys. Res*., *95*, 12,681–12,685, 1990.

Wood, B. J., The effect of H_2O on the 410-kilometer seismic discontinuity, *Science*, *268*, 74–76, 1995.

Wood, B. J., and D. C. Rubie, The effect of alumina on phase transitions at the 660-kilometer discontinuity from Fe-Mg partitioning experiments, *Science*, *273*, 1522–1524, 1996.

Xu, F., J. E. Vidale, P. S. Earle, and H. M. Benz, Mantle discontinuities under southern Africa from precursors to $P'P'_{df}$, *Geophys. Res. Lett*., *25*, 571–574, 1998.

Yamazaki, A., and K. Hirahara, The thickness of upper mantle discontinuities, as inferred from short-period J-Array data, *Geophys. Res. Lett*., *21*, 1811–1814, 1994.

Zhang, Z., and T. Lay, Investigation of upper mantle discontinuities near northwestern Pacific subduction zones using precursors to *sSH*, *J. Geophys. Res*., *98*, 4389–4405, 1993.

G. Helffrich, Earth Sciences, University of Bristol, Wills Memorial Building, Queen's Road, Bristol BS8 1RJ, England. (george@geology.bristol.ac.uk)